ORGANOMETALLICS

pubs.acs.org/Organometallics Article

Homolytic Pd^{II}–C Bond Cleavage in the MILRad Process: Reversibility and Termination Mechanism

Rinaldo Poli,* Dung Nguyen, Yu-Sheng Liu, and Eva Harth*

Cite This: *Organometallics* 2023, 42, 2277–2286 Read Online

ACCESS | Metrics & More | Article Recommendations | Supporting Information

ABSTRACT: This work probed the thermal "switchability" from ethylene coordination/insertion to controlled radical polymerization of methyl acrylate (MA) for Brookhart-type α-diimine Pd^{II} catalysts. The investigation focused on the extremely bulky 2,6-bis(3,5-dimethylphenyl)-4-methylphenyl (Xyl_4Ph) α-diimine *N*-substituents to probe reversible Pd^{II}–C bond activation in the MA-quenched Pd-capped PE intermediate and reversible trapping during radical MA polymerization. The substituent steric effect on the relative stability of various $[PE–MA–Pd^{II}(ArN{=}CMeCMe{=}NAr)]^+$ chain-end structures and on the bond dissociation-free energy (BDFE) for the homolytic Pd^{II}–C bond cleavage has been assessed by DFT calculations at the full quantum mechanics (QM) and QM/molecular mechanics (QM/MM) methods. The structures comprise ester-chelated forms with the Pd atom bonded to the α, β, and γ C atoms as a result of 2,1 MA insertion into the PE–Pd bond and of subsequent chain walking, as well as related monodentate (ring-opened) forms resulting from the addition of MA or acetonitrile. The opened C_α-bonded form is electronically favored for smaller *N*-substituents, including 2,6-diisopropylphenyl (Dipp), particularly when MeCN is added, but the open C_γ-bonded form is preferred for the extremely bulky system with Ar = Xyl_4Ph. The Pd_α–C bond is the weakest one to cleave, with the BDFE decreasing as the Ar steric bulk is increased (31.8, 25.8, and 12.6 kcal mol^{-1} for Ph, Dipp, and Xyl_4Ph, respectively). However, experimental investigations on the $[PE–MA–Pd^{II}(ArN{=}CMeCMe{=}NAr)]^+$ (Ar = Xyl_4Ph) macroinitiator do not show any evidence of radical formation under thermal activation conditions, while photolytic activation produces both TEMPO-trapped (TEMPO = 2,2,6,6-tetramethylpiperidinyloxy) and unsaturated MA-containing PE chains. The DFT investigation has highlighted a low-energy pathway for termination of the PE–$MA^\bullet$ radicals by disproportionation, promoted by β-H elimination/dissociation and H-atom abstraction from the Pd^{II}–H intermediate by a second radical. This phenomenon appears to be the main reason for the failure of this Pd^{II} system to control the radical polymerization of MA by the OMRP (OMRP = organometallic-mediated radical polymerization) mechanism.

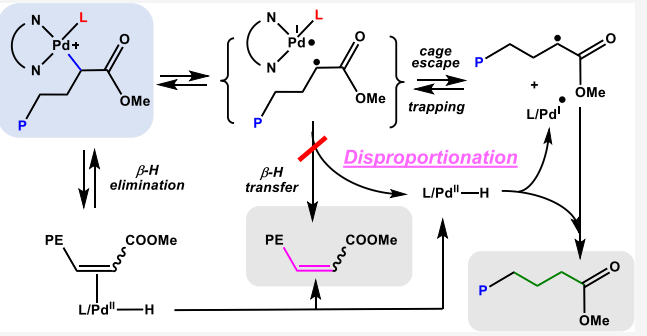

INTRODUCTION

Late-transition-metal polymerization involving Brookhart-type Pd(II) diimine complexes benefits from the unique "chain walking" behavior in which the metal center migrates along the growing polymer chain.[1] This phenomenon is influenced by the nature of diimine ligand substituents and leads to polymers with different branching characteristics and microstructures.[2−7] These catalysts promote the living polymerization of ethylene and α-olefins, and their tolerance to oxygen-containing functionalities also allows the copolymerization of ethylene and polar monomers.[8,9] The insertion of an acrylate and the rearrangement of the resulting chain (**A** in Scheme 1) yields a 6-membered chelate **B** as a stable catalyst resting state and causes a rate retardation together with decreased productivity, which has been attributed to the slow chelate ring opening to yield species **C** (L = monomer). The amount of acrylate has an influence on the stability of chelate **B**. An acrylate excess leads to decomposition, while the complex is stable for days with no excess.[10] The resulting copolymers have lower molar masses than the corresponding olefin homopolymers, with the acrylate functionalities placed at the end of the polymer branches.[10] While the migratory insertion of the electron-deficient methyl acrylate (MA) occurs more rapidly than the insertion of olefins, the low binding affinity of the acrylate monomer leads to the predominant incorporation of the α-olefins.[10]

The ability of the chelate resting state to function as a valuable precursor to form polyolefin radicals as the key intermediate has been investigated in the developed metal-insertion light-initiated radical polymerization (MILRad).[11,12] Here, the resting state (**B**) of Scheme 1 is used to switch from

Received: June 17, 2023
Published: August 10, 2023

https://doi.org/10.1021/acs.organomet.3c00277
Organometallics 2023, 42, 2277−2286

Scheme 1. Chain Walking in Methyl Acrylate/α-Olefin Copolymerization Catalyzed by Cationic (α-Diimine) Pd^{II} Complexes and "Switching" to the Radical Pathway (MILRad) to Form Block Copolymers

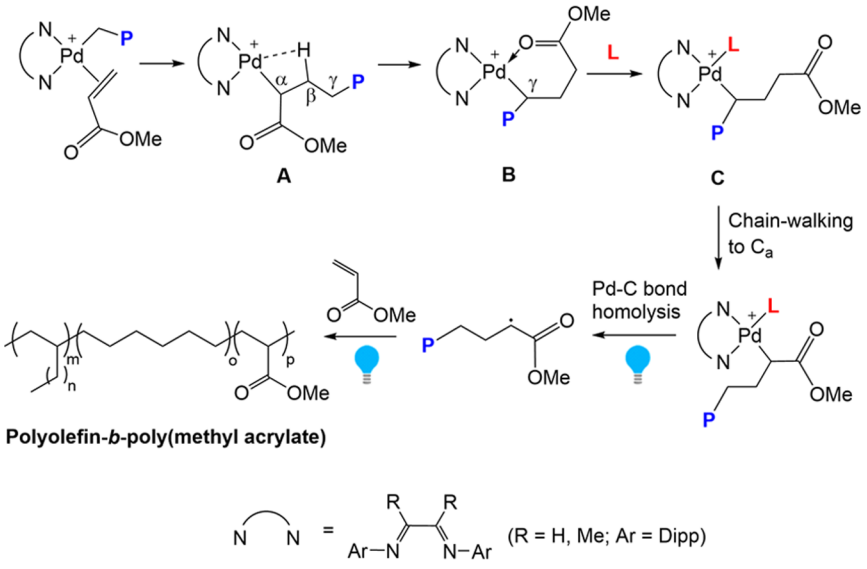

Scheme 2. [Pd(ArN═CMeCMe═NAr)Me(MeCN)]$^+$ Photolysis in the Presence of MA and TEMPO (Ar = Dipp)[13]

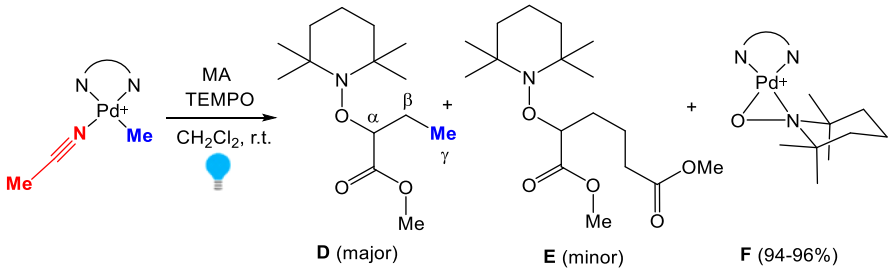

the coordination/insertion to the radical pathway in a one-catalyst system. The presence of an ancillary ligand such as acetonitrile was shown to promote chelate opening, and the Pd−C bond becomes susceptible to homolytic cleavage under light irradiation, which results in the formation of a polyolefin radical, which is able to initiate a free-radical polymerization and form a polyolefin-*b*-polyacrylate block copolymer. A previously reported mechanistic investigation was focused on the reactivity of the chelate, on the identification of macroradicals, and on the initiation of the radical process.[13] Small-molecule models of the 6-membered chelate resting state **B** of Scheme 1, obtained by MA insertion into the Pd−CH_3 bond, have been isolated and characterized, including by single-crystal X-ray diffraction.[14,15]

The formation of [(α-diimine)Pd(TEMPO)]$^+$ (**F**, TEMPO = 2,2,6,6-tetramethylpiperidinyloxy) and TEMPO−CH_3 from the photolysis of [(α-diimine)PdMe(MeCN)]$^+$ in the presence of excess TEMPO indicates the occurrence of a homolytic Pd−Me bond photocleavage with generation of a methyl radical and a Pd^I intermediate.[13] However, when the same experiment was carried out in the presence of MA, only products resulting from the insertion of either one MA molecule into the Pd−CH_3 bond (**D**, Scheme 2) or two MA molecules into the Pd−H bond (**E**) could be identified. Additionally, excess TEMPO captures the Pd^I intermediate to form the [(α-diimine)Pd(TEMPO)]$^+$ complex (**F**) as a byproduct. The near quantitative recovery of **F** suggests a near-quantitative Pd−C bond homolytic cleavage. Since no TEMPO−CH_3 was identified, it can be concluded that MA insertion precedes the bond homolysis.

It is also interesting to note that no isomers of **D** (*i.e.*, with TEMPO bonded to the C_β or C_γ atom) were detected. On the other hand, the minor product **E** results from the insertion of a second MA molecule after chain walking. This suggests that either the Pd−C_α bond is the only one undergoing photocleavage or that the C_α-, C_β-, and C_γ-based radicals easily equilibrate to the thermodynamically more stable C_α-radical prior to TEMPO trapping. The former hypothesis seems consistent with the observation of no photocleavage when the isolated complex [(α-diimine)Pd(κ^2:*C*,*O*-$CH_2CH_2CH_2COOCH_3$)]$^+$ was irradiated in the presence of TEMPO, even in the presence of MA. On the other hand, photocleavage occurs again in the presence of MeCN, at a rate proportional to the MeCN concentration, suggesting that the alkyl radical is generated through photolysis of the open form of the chelate and that the opening process is more easily promoted by MeCN than MA. Finally, after formation of the polyolefin−MA−Pd product (6-membered chelate after chain walking), photolysis in the presence of either MA or MeCN allowed the identification of three different types of TEMPO-terminated chains (Scheme 3), with the TEMPO trap bonded to the C_α (**G**), C_β (**H**), and a more distant C atom (**I**) from the ester group.

One point that remains unclear is whether these three products are derived from different photocleavage processes or from the same Pd−C_α bond photocleavage, followed by radical

https://doi.org/10.1021/acs.organomet.3c00277
Organometallics 2023, 42, 2277−2286

Scheme 3. Photolysis of the [Polyolefin−MA−Pd(ArN═CMeCMe═NAr)]$^+$ in the Presence of MA and TEMPO (Ar = Dipp)

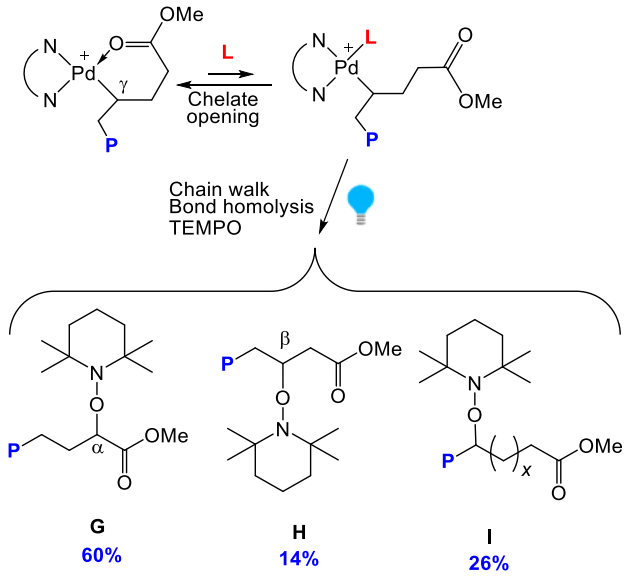

isomerization, with possible intervention of the Pd^I complex that is simultaneously produced by the photocleavage. Indeed, the photocleavage initially produces the organic radical and the Pd^I metalloradical in a radical cage, where chemistry may take place before diffusion. During the MILRad process, the MA radical polymerization does not appear to have the expected characteristics of a controlled process, and the Pd complex ultimately precipitates from the reaction medium as Pd black. However, controlled radical polymerizations by the organometallic route (OMRP, organometallic-mediated radical polymerization)[16−18] have been observed for other mediating metal complexes.[19,20] Another question of interest, therefore, is whether it may be possible to promote reversible radical trapping and a controlled polyacrylate chain growth by ligand engineering, notably by weakening the Pd^{II}−PMA bond, allowing a thermal switch from the coordination/insertion to the radical mechanism.

In order to address these questions, DFT studies were carried out on the chelate ring opening and Pd−C homolytic bond cleavage in the model complexes **1-*α*/*β*/*γ*** (Scheme 4), representing various possible PE−MA−Pd chain ends. These molecules result from the 2,1 insertion of MA into the Pd−Et bond (*i.e.*, the PE chain is simplified with an ethyl group, ***α***) and subsequent chain walking (***β*** and ***γ***). A DFT investigation of the MA insertion and chelate ring-opening steps for the Pd-based "Brookhart" catalyst has previously been reported by Michalak and Ziegler (MZ),[21] but no previous work has assessed the relative homolytic bond strength of various Pd−C bonds for radical initiation, to the best of our knowledge.

Initial full QM studies were conducted on simplified systems with HN═CHCH═NH and PhN═CMeCMe═NPh as the diimine ligand. Subsequently, the substituent effects have been assessed at the QM/MM level on complexes with ArN═CMeCMe═NAr ligands, namely, with Ar = 2,6-diisopropylphenyl (Dipp), previously used in MILRad work,[11−13] and the bulkier 2,6-bis[bis(3,5-dimethylphenyl)methyl]phenyl (henceforth abbreviated as Xyl$_4$Ph),[22] in order to probe a possible thermal activation in the MILRad switching step.

Scheme 4. Systems Investigated in This Work

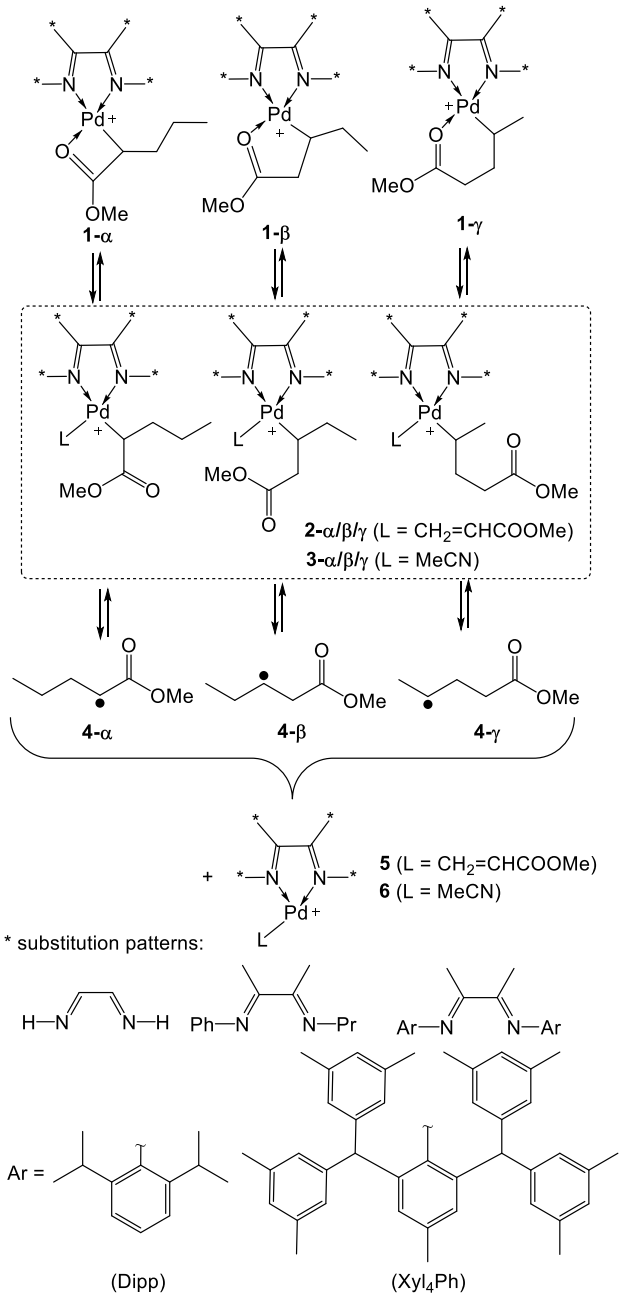

RESULTS AND DISCUSSION

All calculations were carried out at the B3LYP-D3 level. The B3LYP functional was chosen because it was also used in the previous study by MZ. However, we added Grimme's D3 empirical correction for dispersion interactions[23] because its use was shown to considerably improve the performance of this functional in predicting energies, notably BDEs, in benchmarking studies of a variety of organometallic systems.[24] This D3 correction plus a polarizable continuum (SMD approach[25]), to model the effect of dichloromethane solvation, were applied during the geometry optimization. The electronic energies of the optimized geometries were further corrected for thermal and concentration effects to express relative stabilities on the Gibbs energy scale under standard conditions (298.15 K, 1 molar solutions).

https://doi.org/10.1021/acs.organomet.3c00277
Organometallics 2023, 42, 2277−2286

The 2,1 insertion of MA, which is known to be preferred over the 1,2 insertion,[10] into the Pd−polyethylene bond (truncated in our calculations to an ethyl group) initially yields **1-*α***, which transforms by subsequent chain walking steps to **1-*β*** and **1-*γ*** (Scheme 4). Addition of L to each of these systems produces the corresponding adducts (**2-*α*/*β*/*γ***, if L = CH_2═CHCOOMe; **3-*α*/*β*/*γ***, if L = MeCN) and subsequent homolytic cleavage yields the radical **4-*α*/*β*/*γ*** and a 3-coordinate Pd^I complex (L = CH_2═CHCOOMe, **5**; MeCN, **6**).

Among the isomeric organic radicals (**4-*α*/*β*/*γ***), **4-*α*** is calculated as the most stable (**4-*β*** and **4-*γ*** are 5.4 and 5.1 kcal mol^{-1} higher in energy, respectively), as expected because of the unpaired electron delocalization onto the ester carbonyl group. The presence of the fourth C atom (C_δ) renders **4-*β*** and **4-*γ*** (both secondary radicals) energetically equivalent, as seen by comparison with the analogous radicals having one fewer C atom, in which the ***γ*** radical is primary and further destabilized (Figure S2).

(a) QM Study on the HN═CHCH═NH Systems. The calculations on this simplified system (**1-H,*α*/*β*/*γ***) allowed not only to speed up the geometry optimizations but also to evaluate the geometry and relative stability of various systems independent of the bulky diimine substituent steric effect. The results for L = MA are shown in Figure 1. The 6-membered

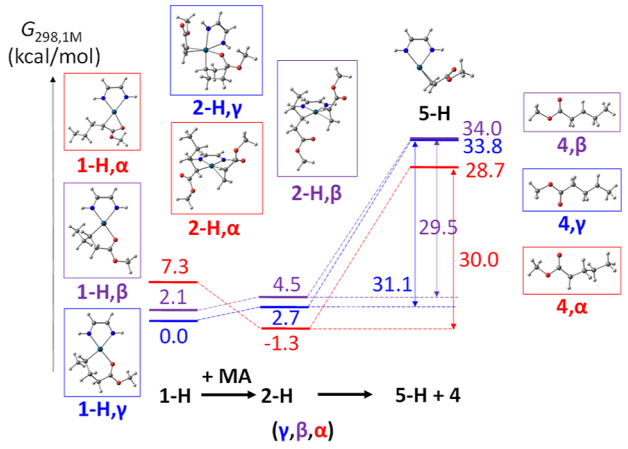

Figure 1. Relative Gibbs energies and views of the optimized geometries for the chelate ring opening by CH_2═CHCOOMe in **1-H,*α*/*β*/*γ*** and of the Pd−C homolytic bond cleavage in **2-H,*α*/*β*/*γ***, yielding **4-*α*/*β*/*γ*** and **5-H**.

chelate (**1-H,*γ***) is the most stable isomer, followed by the 5-membered chelate (**1-H,*β***; 2.1 kcal mol^{-1} higher) and the 4-membered chelate (**1-H,*α***; at 7.3 kcal mol^{-1} from **1-H,*γ***). There is quite good agreement between these results and those previously obtained by MZ[21] on a closely related model (with one additional CH_2 in the alkyl chain, *i.e.*, the product of 2,1-insertion of MA into the Pd $CH_2CH_2CH_3$ bond) for which the 6-, 5-, and 4-membered chelates have relative energies of 0, 1.1, and 7.2 kcal mol^{-1}, respectively. The MA addition is endoergic by 2.7 and 2.4 kcal mol^{-1} for **1-H,*γ*** and **1-H,*β***, respectively, but exoergic by −8.6 kcal mol^{-1} for **1-H,*α***. The optimized structure of **2-H,*γ*** is a trigonal bipyramid with *eq* MA, *ax,eq* diimine, and *ax,eq* chelated alkyl ligand with the ester CO donor in the equatorial site. In the structures of **2-H,*β*** and **2-H,*α***, on the other hand, the ester carbonyl donor has dissociated to yield a square-planar coordination sphere.

These results differ from those of the MZ contribution in terms of both relative energies and geometries, even though the two investigation used the same functional and the models used for the calculation differ only by one CH_2 group in the alkyl chain. In the MZ publication, the MA addition was described as exoergic for all three systems by −11.0, −9.5, and −13.0 kcal mol^{-1}.[21] We believe that this discrepancy is due to the neglect by MZ of solvation, dispersion, and thermal effects (the values given by MZ are gas-phase electronic energies). The entropic penalty for the condensation of two independent molecules to afford a single product molecule easily explains the lower stabilization computed in our investigation. Indeed, on the electronic energy scale, the MA addition to **1-H,*α*/*β*/*γ*** yields changes of −9.7/−10.4/−20.6, in better agreement with the previously reported ones. In addition, as outlined above, our results compare quite well with those of the previous investigation in terms of the relative energies of the **1-H,*α*/*β*/*γ*** isomers, where solvation, dispersion, and thermal corrections are expected to be quite similar.

Rationalization of the structural differences between our optimized structures and those of the MZ investigation is subtler. The same optimized geometry has been obtained only for the 6-membered chelate isomer. The CH_2 homologues of **2-H,*β*** and **2-H,*α*** optimized by MZ were also chelated, 5-coordinated geometries[21] (see a detailed comparison in Figure S3). In order to get further insights into the reason of this difference, the **2-H,*β*** and **2-H,*α*** geometries were reoptimized with removal of either the dispersion or the solvation correction, or both. As shown in Figure S4, the removal of either correction strengthens the Pd←O═C interaction for the **2-H,*β*** structure, restoring a 5-coordinate geometry close to that observed for the CH_2 homologue in the previous study.[21] For the structure of **2-H,*α***, on the other hand, a square-planar environment was obtained under all approximation. It is important to underline that all these optimizations were run using 5-coordinate guess geometries derived from those optimized by MZ. The localized 5-coordinate minimum with a very strained 4-membered chelate for the CH_2 homologue (Figure S3) probably results from the different choice of basis set. In all evidence, the Pd←O═C interaction is very weak and can be broken by any minor perturbation.

The results shown in Figure 1 suggest that, although the Pd-capped PE chain obtained after quenching with MA is most stable after chain walking to the 6-membered chelate, the chelate can open and chain-walk back to the primary insertion product, with the Pd atom bonded to the C_α atom in an MA-rich environment.

The next step of the MILRad switch is the homolytic Pd−C bond cleavage. The resulting 3-coordinate Pd^I complex (**5-H**) exhibits a T-conformation, as experimentally observed in isolated complexes with bulky ligands, *e.g.*, [$PdCl(C_6H_5$-4-F)(PAd_3)] (Ad = 1-adamantyl)[26] and $[Pd(CH_3)(PtBu_3)_2]^+$.[27] The relative stability trend of **2-H,*α*/*β*/*γ*** is very similar to that of **4-*α*/*β*/*γ***, yielding very similar bond dissociation Gibbs energies (BDGE) for the three systems. These BDGE values (in the 29.5−31.1 kcal mol^{-1} range) are slightly lower than that calculated for the Pd−CH_3 bond in $[Pd(HN{=}CHCH{=}NH)(CH_3)(MA)]^+$ (36.1 kcal mol^{-1}) but still too high for a facile thermal activation,[28,29] hence dissociation only occurs upon photolytic activation. Note that the computed relative energies indicate that the various opened PE−MA−Pd isomeric chains would be present with a thermal distribution qualitatively matching the observed distribution of TEMPO-

https://doi.org/10.1021/acs.organomet.3c00277
Organometallics 2023, 42, 2277−2286

trapped chains in the experimental investigation.[13] This suggests that each observed product may be directly derived from the photocleavage of the corresponding Pd−C bond.

The results of the ring-opening and Pd−C bond cleavage processes for L = MeCN are shown in Figure 2. The relevant

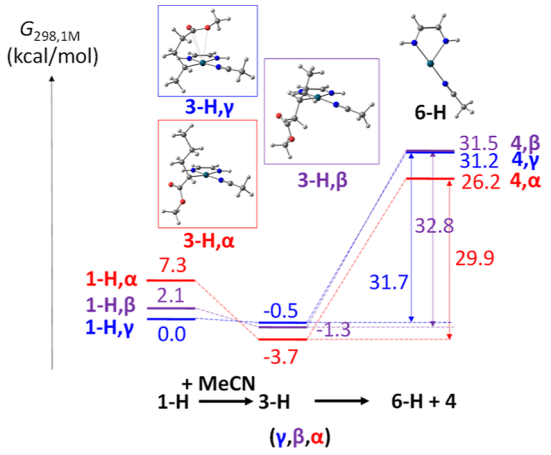

Figure 2. Relative Gibbs energies and views of the optimized geometries for the chelate ring opening by MeCN in **1-H,*α*/*β*/*γ*** and of the Pd−C homolytic bond cleavage in **3-H,*α*/*β*/*γ***, yielding **4-*α*/*β*/*γ*** and **6-H**.

differences with respect to the MA additions are as follows. The Pd−L bond formation provides greater stabilization for MeCN than for MA: all chelate opening processes are now exoergic. All **3-H,*α*/*β*/*γ*** products adopt a square-planar configuration. However, whereas the ester carbon chain adopts the most favorable all-anti conformation for the CCCC dihedral angles in **3-H,*α*** and **3-H,*β***, the optimized geometry of **3-H,*γ*** features the ester group bending over the axial position, oriented in a parallel fashion to the coordination plane, with long Pd···(O−C═O) distances (Pd···C = 3.14 Å; Pd···O = 3.40, 3.44 Å). This suggests a weak n−π interaction involving the Pd d_{z^2} electrons and the CO_2 π^* orbital. An all-anti geometry for **3-H,*γ*** is 3.3 kcal mol^{-1} higher in energy. The different binding preference for the alkyl ligand in **2-H,*γ*** and **3-H,*γ*** probably derives from the different nature of the ligand−Pd interaction: MeCN is a strong σ donor, thus the Pd d_{z^2} orbital is increased in energy, favoring the interaction with the CO π^* orbital, whereas the π acidic properties of MA render the Pd atom more susceptible to accept the electron density from the O lone pair of the ester carbonyl group. The relative stability of the **3-H,*α*/*β*/*γ*** isomers is similar to that of the **2-H,*α*/*β*/*γ*** isomers, in favor of Pd binding to C_α. However, **3-H,*β*** is now marginally more stable that **3-H,*α***. Anyhow, under kinetically controlled conditions (facile chain walking), the predominant resting state of the PE−MA−Pd chains in an MeCN-rich environment contains a Pd−C bond to the C_α atom. The homolytic Pd−C BDGE values are quite similar to those obtained for the MA-ring-opened systems and slightly lower than that of the Pd−CH_3 bond in [Pd(HN═CHCH═NH)(CH_3)(MeCN)]$^+$ (36.7 kcal mol^{-1}).

(b) Comparative QM and QM/MM Studies on the PhN═CMeCMe═NPh Systems. Before addressing the effect of the bulky aryl groups on the ring opening and homolytic cleavage steps, which could only be handled in a reasonable time frame at the QM/MM level, the effect of the QM/MM approximation was assessed on the intermediate-size PhN═CMeCMe═NPh system, where full QM optimization could also be carried out at a relatively low computational cost. This comparative study was limited to one ring-opening process, from the 6-membered chelate (**1-Ph,*γ***) with only one ligand (MeCN) and with a shorter alkyl chain ($CH_2CH_2CH_2COOMe$). The cutoff between the QM and the MM layers was placed at the level of the N−Ph bonds (the imine CH_3 groups were maintained in the QM layer). The results are shown in Figure 3.

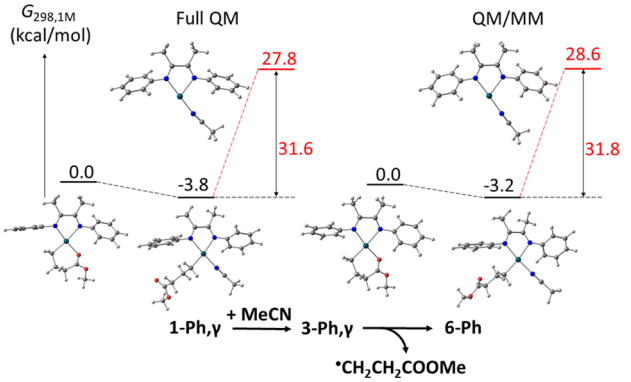

Figure 3. Relative Gibbs energies and views of the optimized geometries for the QM and QM/MM calculations of the chelate ring opening by MeCN in **1-Ph,*γ*** and of the Pd−C homolytic bond cleavage in **3-H,*γ***, yielding **4-*γ*** and **6-Ph**.

A quick glance at the figure shows that the QM/MM approximation is indeed acceptable. It is of interest, however, to comment on a few points. The different computational level has a slight effect on the torsional angles at the N−Ph junction and on the coordination sphere planarity, as can be appreciated in Figure S5. The dihedral angles between the N−Pd−N plane and the C−Pd−O plane (in **1-Ph,*γ***) or C−Pd−NCMe plane (in **3-Ph,*γ***) are 2.6 and 3.6° at the QM level and 15.0 and 16.5° at the QM/MM level. However, these structural changes have no obvious repercussions on the relative energies of the processes being considered here. The chelate ring opening is more favorable for **1-Ph,*γ*** than for **1-H,*γ*** even though the alkyl chain is placed in the all-anti conformation (the more stable conformation found for **3-H,*γ*** with the axial Pd···O_2C interaction was not investigated). The Pd−C homolytic cleavage entails a BDGE close to those of **2-H,*γ*** (Figure 1) and **3-H,*γ*** (Figure 2), hence the imine Ph substituents do not induce any significant steric pressure on the Pd−C bond.

(c) QM/MM Studies on the ArN═CMeCMe═NAr Systems. These calculations followed the same procedure presented in the previous section for the PhN═CMeCMe═NPh ligand system (the imine Ar groups were treated at the MM level, and all other atoms were in the QM layer). Only **1-Ar,*γ*** was considered among all **1-Ar** isomers, and the ligand addition was once again restricted to MeCN, but all chain-walking isomers were considered for the ring-opened structure (**3-Ar,*α*/*β*/*γ***). The Gibbs energy changes obtained for Ar = Dipp and Xyl_4Ph are shown in Figure 4, while the geometries are shown in the Supporting Information (Figures S6 and S7, respectively).

The steric encumbrance increase (Ph < Dipp < Xyl_4Ph) has several notable effects. The first one is a destabilization of the opened isomers (**3-Ar,*α*/*β*/*γ***) relative to the 6-membered chelate complex (**1-Ar,*γ***). While the ring opening to yield **3-**

https://doi.org/10.1021/acs.organomet.3c00277
Organometallics 2023, 42, 2277−2286

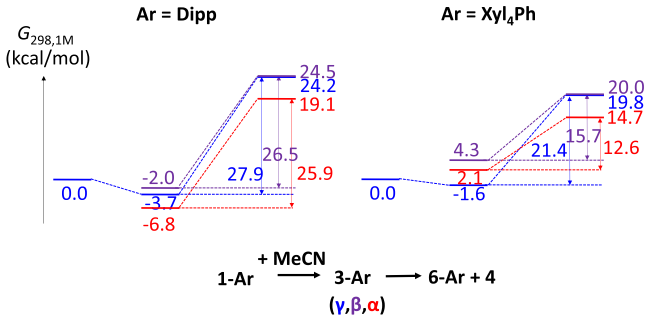

Figure 4. Relative Gibbs energies for the QM/MM calculations of the chelate ring opening by MeCN in **1-Ar,*γ*** and of the Pd−C homolytic bond cleavage in **3-Ar,*α*/*β*/*γ***, yielding **4-*α*/*β*/*γ*** and **6-Ar** (Ar = Dipp, left; Xyl_4Ph, right).

Ar,*γ* from **1-Ar** + MeCN yields approximately the same Gibbs energy change for Ar = Ph (−3.2 kcal mol^{-1}, Figure 3) and Dipp (−3.7 kcal mol^{-1}, Figure 4), the stabilization is reduced for the bulkier Xyl_4Ph system. Further, while **3-Ar,*α*** remains the most stable isomer for Ar = Dipp, the Gibbs energy of this isomer is increased above that of **3-Ar,*γ*** for Ar = Xyl_4Ph. Isomer **3-Ar,*β*** is likewise increased in energy for the bulkier system. These effects are related to the steric limitations imposed by the Ar substituents, as can be appreciated from Figures S6 and S7. An indication of this steric effect is given by the distortion of the square-planar coordination geometry, as judged from the dihedral angle between the PdN_2 (imine) plane and the CPdX plane, where X is O for **1** and N (MeCN) for **3**, even though this distortion may be overestimated. The most important result is that the equilibrium distribution of the possible isomeric forms of the PE−MA−Pd resting state is ligand-dependent, with greater steric bulk skewing the distribution, disfavoring the most congested isomer with Pd bonded to C_α.

Finally, perhaps the most important effect of the increased Ar steric bulk is the drastic decrease of the Pd−C BDGE, dropping from the 29.9−32.8 kcal mol^{-1} range for the non-congested system (H) to the 25.9−27.9 kcal mol^{-1} range for the Ar = Dipp system and to the 12.6−21.4 kcal mol^{-1} range for the Ar = Xyl_4Ph system. This decrease is paralleled by a small but significant increase of the Pd−C distance, see Table S1. The Pd−C distances for the less encumbering system (X = H) are similar to those of the corresponding Dipp systems and thus do not fit into the steric trend. This is probably due to an electronic effect related to the difference between the N−H and N−Ar (Ar = Ph, Dipp, and Xyl_4Ph) bonds.

In conclusion, while the Pd−C strength is large enough to ensure radical trapping of the growing PE-*b*-PMA$^\bullet$ radical chain, generated by the MILRad switch and MA incorporation, by L/Pd^I for all ligand systems, potentially leading to OMRP under light irradiation conditions, the BDGE values calculated for the **Xyl_4Ph** system are low enough to envisage a possible thermal activation and a controlled radical polymerization by the OMRP mechanism under thermal conditions.

(d) Experimental Investigation of MILRad for Ar = Xyl_4Ph. On the basis of the above suggestion, a living [PE−MA−Pd(ArN═CMeCMe═NAr)]$^+$ polymer with Ar = Xyl_4Ph was synthesized and investigated as a macroinitiator for the free-radical polymerization of MA under both thermal and photochemical activation conditions. Specifically, homopolymerization of MA was initially tested at three different temperatures (25, 50, and 80 °C) in the absence of blue light (Supporting Information). Over the period of 48 h, none of the reactions resulted in the formation of any PMA. The same result was obtained after introduction of MeCN to facilitate chelate ring opening. Notably, significant catalyst degradation occurred at 80 °C, leading to the formation of a substantial amount of palladium black after 24 h. This indicates that the Xyl_4Ph system exhibits poor thermal stability at elevated temperatures.

TEMPO-trapping experiments were conducted after both light activation (room temperature) and thermal activation (50 °C) of the [PE−MA−Pd(ArN═CMeCMe═NAr)]$^+$ macroinitiator in the presence of MA. The thermal activation produced only PE chains, functionalized by MA at the chain-end, without any TEMPO trapping. The unsaturated chains are clearly evidenced in the ^1H NMR spectrum (Figure 5A and

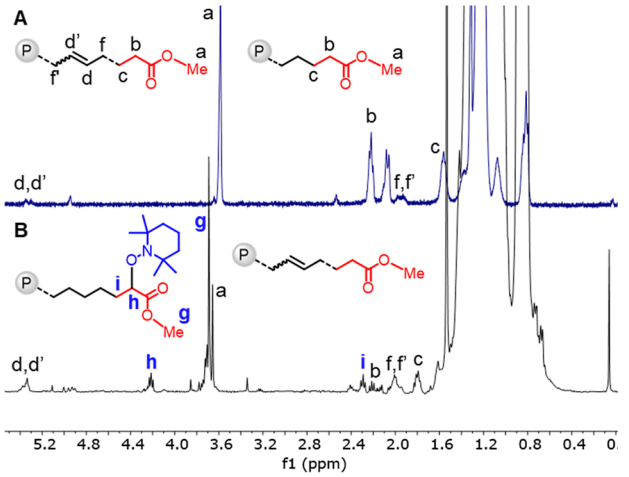

Figure 5. (A) ^1H NMR spectrum of chain-end-functionalized PE−MA obtained *via* thermal activation. (B) ^1H NMR spectrum of TEMPO-trapped PE−MA−TEMPO obtained *via* light activation.

full spectrum in Figure S8) by the sp^2-CH resonances at *ca.* 5.4 ppm (d, d′). These chains may be produced by *β*-H elimination/chain-walking/dissociation. The Pd−H complex left behind can then either deliver the hydride in a non-radical pathway to another [PE−MA−Pd(ArN═CMeCMe═NAr)]$^+$ macroinitiator to produce saturated chains (which would contribute to resonances b and c), or release H_2 (undetected) during the thermal decomposition to Pd black. This strongly suggests that thermal activation cannot operate the switch to a radical process and that the catalyst degrades at elevated temperatures without undergoing Pd−C bond homolysis.

Light activation, on the other hand, produced TEMPO-trapped PE with only one MA monomer at the chain end, in which the characteristic methine proton was detected at 4.2 ppm (resonance h) and the ester Me resonance at 3.7 ppm (g), see Figure 5B and full spectrum in Figure S9. However, unsaturated chains were also formed under these conditions (resonances a, b, c, d, d′, f, and f′). Since the [PE−MA−Pd(ArN═CMeCMe═NAr)]$^+$ intermediate does not spontaneously decompose at this temperature without light irradiation, these chains may only be produced, together with the Pd^{II}−H complex, by a light-induced *β*-H elimination. Namely, light irradiation may favor dissociation of the chelated carbonyl donor function. An alternative possibility to generate the same products is a *β*-H atom transfer within the caged radical pair, {L/Pd^I,$^\bullet$MA−PE}, prior to radical diffusion and

https://doi.org/10.1021/acs.organomet.3c00277
Organometallics 2023, 42, 2277−2286

Scheme 5. Possible Pathways of Pd-Mediated Polyacrylate Radical Disproportionation

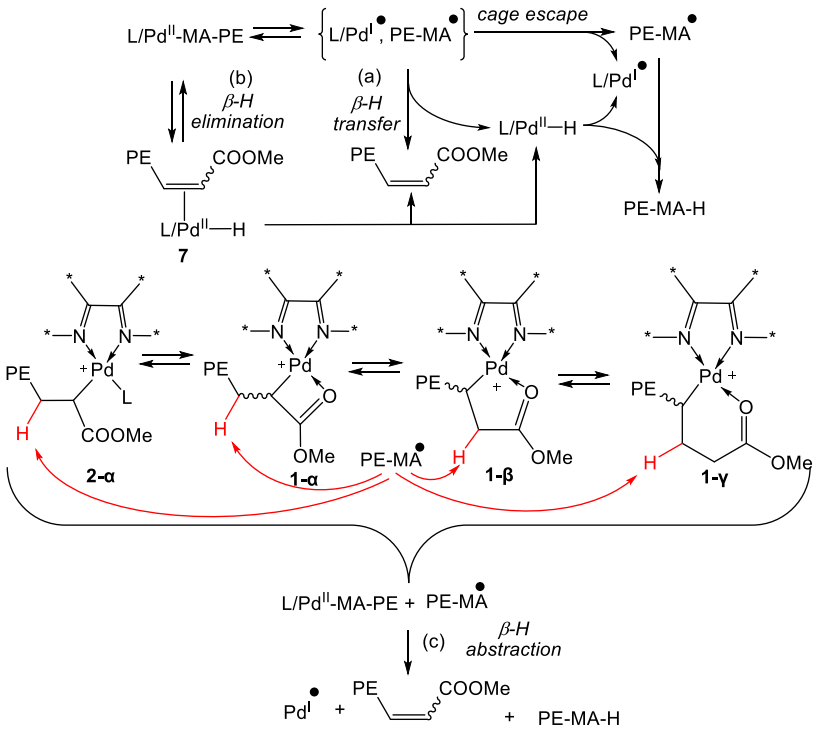

TEMPO trapping. On the other hand, the Xyl_4Ph system was demonstrated to readily undergo the MILRad process to produce high-molecular-weight PMA in the absence of TEMPO,[22] which further suggests that light irradiation is the only mode of activation for MILRad. The radical process, however, did not show any sign of control,[22] producing terminated chains that most probably result, as demonstrated for the Dipp system,[13] from disproportionation.

(e) Pd-Catalyzed Acrylate Radical Disproportionation. The MILRad process for the Dipp system was reported to ultimately yield chains terminated solely by disproportionation.[13] However, it has long been established[30−32] and recently confirmed[33] that the spontaneous bimolecular acrylate radical termination occurs predominantly by combination, with a negligible (unobserved) contribution of disproportionation. A report revealing the exclusive disproportionation of polyacrylate radicals, resulting from the photochemical activation of tellanyl-terminated narrow-dispersity chains obtained by TERP,[34] was later suggested to result from a tellurium-mediated two-step process, whereby the tellanyl radical in the caged {RTe$^\bullet$,polyacrylate$^\bullet$} radical pair abstracts the β-H atom from the polymer chain end to yield a transient RTeH intermediate, which then delivers the H atom to a second radical chain.[35] As suggested in previous section, the same type of reactivity may be responsible for the generation of unsaturated chains upon photoactivation of the [PE−MA−Pd(ArN═CMeCMe═NAr)]$^+$ (Ar = Xyl_4Ph) macroinitiator (Figure 5B). Consequently, we probed the possible action of the spin doublet Pd^I complex **5** in a similar Pd^I-mediated disproportionation process. This action is illustrated in Scheme 5 (path a): after homolytic bond cleavage, β-H atom transfer within the caged radical pair would yield the unsaturated polymer chain and L/Pd^{II}−H. Subsequently, H atom transfer from this hydride intermediate to an escaped radical would generate the second product of radical disproportionation, the saturated chain, and a second L/Pd^I complex. The DFT investigation, however, did not support the occurrence of this pathway. The reason is that the Pd^I complex within the caged radical pair does not easily abstract the β-H atom from the organic radical; the Pd···β-H approach rather leads to a higher-energy 5-coordinate geometry with the organic radical linked to the metal center *via* the ester carbonyl function (full details of these calculations are provided in the Supporting Information).

An alternative possibility (Scheme 5, path b) for the Pd-mediated disproportionation starts with β-H elimination, yielding directly, without homolytic bond cleavage, a Pd hydride complex **7** in which the unsaturated chain is part of the coordination sphere. The latter may dissociate either prior to (as shown in Scheme 5) or after the H atom transfer from the hydride complex to a radical chain, generated by homolytic bond cleavage, as in path a. Yet another possibility consists of abstraction, by the free-radical chain, of a β-H-atom from the Pd-bonded polymer chain (Scheme 5, path c). This may occur for either the κ^1-bonded chain (*e.g.*, complexes **2-*α*/*β*/*γ***; for simplicity, only **2-*α*** is shown in the scheme), or from one of the chelated forms (**1-*α*/*β*/*γ***), to simultaneously produce the saturated and unsaturated chains. Note that only the β-H-atom abstractions from **1-*α*/*β*** and **2-*α*/*β*** would produce an unsaturated chain where the C═C unsaturation is conjugated with the ester group, whereas abstraction from the chain-walked **1-*γ*** and **2-*γ*** would lead to a non-conjugated unsaturated chain.

The DFT investigation has considered both pathways b and c, though the latter was restricted to the chelated complexes **1-*α*** and **1-*β***. These calculations were carried out at the full QM level on the H-substituted diimine system and both coordinated and free-radical alkyls were simplified to $CH_3CH_2CH(COOCH_3)$, for computational efficiency. The results are collected in Figure 6.

https://doi.org/10.1021/acs.organomet.3c00277
Organometallics 2023, 42, 2277−2286

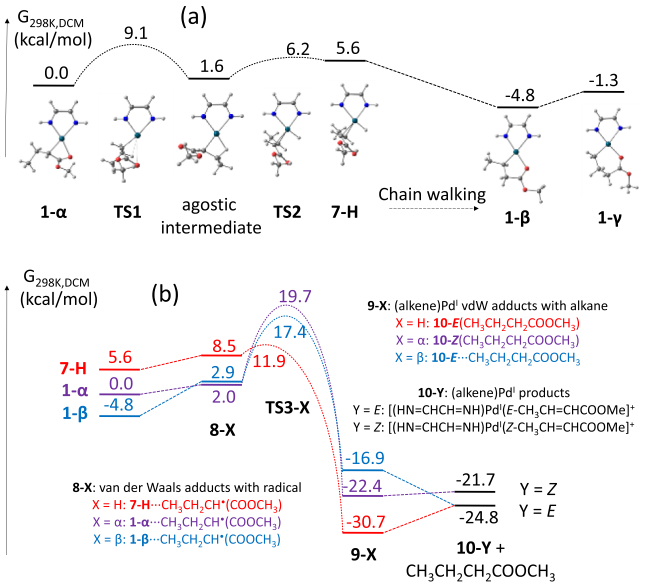

Figure 6. Gibbs energy profile for the (a) β-H elimination process leading from **1-H,*α*** to **7-H** and (b) H-atom abstraction from the hydride complex **7-H** and from the chelated complexes **1-H,*α*** and **1-H,*β***.

As shown in Figure 6a, the rearrangement of **1-H,*α*** to **7-H** is quite facile, as expected from the experimental observation of a rapid chain-walking process. The rate-determining step is the initial associative substitution of the chelated carbonyl group by the β-CH bond *via* **TS1**, to yield the agostic intermediate in preparation for the β-H elimination step. The latter has a very small barrier *via* **TS2**, which is late, with geometry and energy very close to those of the final hydride complex **7-H**. The stereochemistry of the generated alkene ligand, $CH_3CH{=}CHCOOCH_3$, is *E*. The barriers of the subsequent chain-walking steps to generate **1-H,*β*** and **1-H,*γ*** were not explored.

Starting from **7-H**, the radical addition first yields a van der Waals adduct (Figure 6b, red path), with a very low Gibbs energy cost due to the entropic penalty, while the interaction is exoenthalpic. The H-atom abstraction then proceeds with a quite low barrier through **TS3-H**, at 6.3 kcal mol^{-1} relative to **7-H** and 11.9 kcal mol^{-1} relative to **1-H,*α***, ending up in a local minimum **9-H**, which is a square-planar Pd^{I} complex in which the alkane product, $CH_3CH_2CH_2COOCH_3$, remains coordinated *via* the ester OCH_3 function. The O−Pd interaction is, however, rather weak, and the alkane product can easily dissociate to produce the T-shaped three-coordinate Pd^{I} complex **10-*E***. Views of all optimized geometries along this path are available in the Supporting Information (Figure S14).

The alternative H-atom abstraction processes starting from **1-H,*α*** and **1-H,*β*** (violet and blue paths in Figure 6b, respectively) proceed *via* the same type of intermediates, but the barriers from the vdW adducts **8-X** (X = α or β) are much higher. This is certainly related to the greater bond strength of the C−H bond being broken, relative to the Pd−H bond in **7-H**, which is not sufficiently compensated by the forming CH bond in the saturated organic product. The geometries of the **TS3-*α*** and **TS3-*β*** transition states (Figure S14) show considerable lengthening of the C−H bond being cleaved (>0.2 Å from *ca.* 1.09 to >1.3 Å) and the near equivalence of the two C···H distances, whereas the Pd−H distance in **TS3-H** (1.535 Å) is only 0.015 Å longer than in the **7-H** precursor. For this reason, we believe that the corresponding H-atom abstractions from **1-H,*γ*** and from **2-H,*α*/*β*/*γ*** should also feature high barriers and would not be competitive with the pathway from **7-H**. The H-atom abstraction from **1-H,*α*** leads to a **9-*α*** complex that, like **9-H**, maintains the saturated organic product linked *via* the ester OCH_3 function in the coordination sphere. Interestingly, the unsaturated organic product, with a *Z* stereochemistry, is coordinated *via* the ester carbonyl function in this intermediate, whereas the unsaturated *E* organic molecule in the equivalent **9-H** binds *via* the C=C function. Dissociation of the saturated organic ligand yields a T-shaped product **10-*Z***. The atom abstraction from **1-H,*β***, on the other hand, produces a **9-*β*** intermediate where the saturated organic product is in the outer sphere and the unsaturated organic product has an *E* stereochemistry and binds *via* the C=C function, like in the T-shaped **10-*E*** Pd^{I} complex.

In conclusion, after homolytic Pd^{II}−MA−PE bond breaking, the produced PE−MA$^{\bullet}$ radical most likely interacts with an L/Pd^{II}−H intermediate, which is in dynamic equilibrium with the Pd-capped polymer dormant species, leading to terminated chains that are equivalent to those of a radical disproportionation process. The mechanism, however, does not follow a radical disproportionation pathway but is rather assisted by a classical 2-electron β-H elimination in the polymer dormant species, which yields a more readily extractable H atom. Although this mechanism easily accounts for disproportionation by photolytic activation of the Pd-bonded PE−MA chains, further considerations must be made to explain the observed disproportionation during the MA radical polymerization for the MILRad process with the Dipp system[13] because the chain grows in the free radical form and because the calculations have shown the reluctance of Pd^{I} to abstract a β-H atom next to the ester carbonyl function in the free-radical chain (see the Supporting Information). However, the Pd^{I} complex is perfectly able to trap the radical at the C atom to regenerate a Pd-capped chain (PE-*b*-PMA−Pd^{II}/L), which can then proceed by β-H elimination to yield the unsaturated termination product and the hydride intermediate. This radical trapping should be quite favorable, according to the calculated bond dissociation free energy (BDFE) values, even for the extremely bulky Xyl_4Ph system, and its reversibility is ensured by the photolytic activation, whereas no cleavage occurs under thermal activation. However, the reversibility of the Pd^{II}−C cleavage process is not sufficient to sustain a controlled polymer growth by the OMRP mechanism.[16−18] This outcome is, indeed, the probable consequence of a prevailing Pd-mediated disproportionation, which stoichiometrically reduces the Pd^{II} mediator to Pd^{0}.

This Pd-mediated disproportionation pathway is favored relative to the standard bimolecular termination, which would occur predominantly by combination,[33] because it follows the rate law $v = k_{t,Pd}$[polymer−MA$^{\bullet}$][7], whereas the bimolecular termination follows the law $v = k_t$[polymer−MA$^{\bullet}$]^2 and [7] ≫ [polymer−MA$^{\bullet}$], at least for systems with a not too sterically encumbering α-diimine ligand, which feature high activation barriers for the Pd^{II}−MA−PE homolytic bond cleavage. In addition, the experimental results reported here for the Xyl_4Ph system indicate that, even for this highly congested system in which the Pd^{II}−C bond cleavage has a much reduced BDFE, β-H elimination/chain walking/dissociation is still favored relative to homolytic bond cleavage. Thus, the free-radical flow is much smaller than the dynamic equilibrium concentration of **7**.

https://doi.org/10.1021/acs.organomet.3c00277
Organometallics 2023, 42, 2277−2286

CONCLUSIONS

This contribution has computationally addressed the steric effect of the α-diimine *N*-substituents on the relative stability of various chain-walked chelated structures, as well as ring-opened structures resulting from the addition of MA and acetonitrile, for the metallated chain-end of an MA-quenched living polyethylene chain, [PE−MA−Pd^{II}(ArN═CMeCMe═NAr)]$^+$, obtained with Brookhart-type catalysts. The main point of interest was the "switchability" from coordination/insertion to a controlled radical polymerization process by the OMRP mechanism in the MILRad polymerization, to probe whether reversibility for the Pd^{II}−C homolytic cleavage could be achieved, allowing the eventual formation of controlled olefin-acrylate block copolymers. It was specifically hoped that the steric pressure of the extremely bulky 2,6-bis(3,5-dimethylphenyl)-4-methylphenyl (Xyl_4Ph) substituents would labilize the Pd^{II}−C bond in the intermediate MA-quenched Pd-capped PE chain, allowing thermal activation and reversible radical trapping during the radical MA polymerization process. Indeed, a pronounced steric labilization occurs according to the QM/MM calculations. However, the labilization is still insufficient to generate the PE−MA$^\bullet$ radical by thermal activation of the [PE−MA−Pd^{II}(ArN═CMeCMe═NAr)]$^+$ macroinitiator, while photolytic activation results in a successful switch but still without control for the radical chain growth because of terminations by disproportionation. The computed Pd−C BDFE values indicate that the photogenerated L/Pd^I complex is clearly competent to trap the growing PE-*b*-PMA$^\bullet$ chain, but the lack of control results from a Pd-induced radical termination. This is not a catalyzed radical termination (CRT),[36] as in copper-mediated atom-transfer radical polymerization where the L/Cu^I catalyst is regenerated by the radical termination process.[37−40] It is a stoichiometric process because each termination event irreversibly converts two Pd^{II} centers into two Pd^I centers, ultimately leading to the generation of Pd^0. The present investigation has also unveiled a new way for acrylate radicals to terminate by disproportionation by the mediating action of a transition metal: the unsaturated product is generated by a sequence of radical trapping/β-H elimination/dissociation, operated in this case by the L/Pd^I system that is simultaneously converted into L/Pd^{II}−H, while the saturated product is generated by the subsequent abstraction of the H atom from this intermediate hydride complex by a second radical.

ASSOCIATED CONTENT

Supporting Information

The Supporting Information is available free of charge at https://pubs.acs.org/doi/10.1021/acs.organomet.3c00277.

Experimental and computational details (PDF)

Cartesian coordinates of all optimized geometries (XYZ)

AUTHOR INFORMATION

Corresponding Authors

Rinaldo Poli − *CNRS, LCC (Laboratoire de Chimie de Coordination), UPS, INPT, Université de Toulouse, 31077 Toulouse Cedex 4, France; Institut Universitaire de France, 75231 Paris, France;* orcid.org/0000-0002-5220-2515; Email: rinaldo.poli@lcc-toulouse.fr

Eva Harth − *Department of Chemistry, Center of Excellence in Polymer Chemistry (CEPC), University of Houston, Houston 77004 Texas, United States*; Email: harth@uh.edu

Authors

Dung Nguyen − *Department of Chemistry, Center of Excellence in Polymer Chemistry (CEPC), University of Houston, Houston 77004 Texas, United States*

Yu-Sheng Liu − *Department of Chemistry, Center of Excellence in Polymer Chemistry (CEPC), University of Houston, Houston 77004 Texas, United States*

Complete contact information is available at: https://pubs.acs.org/10.1021/acs.organomet.3c00277

Notes

The authors declare no competing financial interest.

ACKNOWLEDGMENTS

The authors E.H., D.N., and Y.-S.L., thank the Robert A. Welch Foundation for funding (H-E-0041 and E-2066-202110327) through the Center of Excellence in Polymer Chemistry and acknowledge the National Science Foundation (CHEM-2108576) for supporting part of this work. R.P. thanks the CALMIP Mesocenter of the University of Toulouse for the allocation of computational resources.

REFERENCES

(1) Johnson, L. K.; Killian, C. M.; Brookhart, M. New Pd(II)- and Ni(II)-based catalysts for polymerization of ethylene and a-olefins. *J. Am. Chem. Soc.* **1995**, *117*, 6414−6415.

(2) Johnson, L. K.; Mecking, S.; Brookhart, M. Copolymerization of Ethylene and Propylene with Functionalized Vinyl Monomers by Palladium(II) Catalysts. *J. Am. Chem. Soc.* **1996**, *118*, 267−268.

(3) Tempel, D. J.; Johnson, L. K.; Huff, R. L.; White, P. S.; Brookhart, M. Mechanistic studies of Pd(II)-alpha-diimine-catalyzed olefin polymerizations. *J. Am. Chem. Soc.* **2000**, *122*, 6686−6700.

(4) Allen, K. E.; Campos, J.; Daugulis, O.; Brookhart, M. Living Polymerization of Ethylene and Copolymerization of Ethylene/Methyl Acrylate Using "Sandwich" Diimine Palladium Catalysts. *ACS Catal.* **2015**, *5*, 456−464.

(5) Dai, S. Y.; Sui, X. L.; Chen, C. L. Highly Robust Palladium(II) alpha-Diimine Catalysts for Slow-Chain-Walking Polymerization of Ethylene and Copolymerization with Methyl Acrylate. *Angew. Chem., Int. Ed.* **2015**, *54*, 9948−9953.

(6) Dai, S.; Chen, C. Direct Synthesis of Functionalized High-Molecular-Weight Polyethylene by Copolymerization of Ethylene with Polar Monomers. *Angew. Chem., Int. Ed.* **2016**, *55*, 13281−13285.

(7) Zhang, Y. X.; Wang, C. Q.; Mecking, S.; Jian, Z. B. Ultrahigh Branching of Main-Chain-Functionalized Polyethylenes by Inverted Insertion Selectivity. *Angew. Chem., Int. Ed.* **2020**, *59*, 14296−14302.

(8) Tan, C.; Chen, C. Emerging Palladium and Nickel Catalysts for Copolymerization of Olefins with Polar Monomers. *Angew. Chem., Int. Ed.* **2019**, *58*, 7192−7200.

(9) Wang, F. Z.; Chen, C. L. A continuing legend: the Brookhart-type alpha-diimine nickel and palladium catalysts. *Polym. Chem.* **2019**, *10*, 2354−2369.

(10) Mecking, S.; Johnson, L. K.; Wang, L.; Brookhart, M. Mechanistic Studies of the Palladium-Catalyzed Copolymerization of Ethylene and a-Olefins with Methyl Acrylate. *J. Am. Chem. Soc.* **1998**, *120*, 888−899.

(11) Keyes, A.; Basbug Alhan, H. E.; Ha, U.; Liu, Y. S.; Smith, S. K.; Teets, T. S.; Beezer, D. B.; Harth, E. Light as a Catalytic Switch for Block Copolymer Architectures: Metal-Organic Insertion/Light Initiated Radical (MILRad) Polymerization. *Macromolecules* **2018**, *51*, 7224−7232.

(12) Keyes, A.; Dau, H.; Basbug Alhan, H. E.; Ha, U.; Ordonez, E.; Jones, G. R.; Liu, Y. S.; Tsogtgerel, E.; Loftin, B.; Wen, Z. L.; et al. Metal-organic insertion light initiated radical (MILRad) polymerization: photo-initiated radical polymerization of vinyl polar monomers with various palladium diimine catalysts. *Polym. Chem.* **2019**, *10*, 3040−3047.
(13) Dau, H.; Keyes, A.; Basbug Alhan, H. E.; Ordonez, E.; Tsogtgerel, E.; Gies, A. P.; Auyeung, E.; Zhou, Z.; Maity, A.; Das, A.; et al. Dual Polymerization Pathway for Polyolefin-Polar Block Copolymer Synthesis via MILRad: Mechanism and Scope. *J. Am. Chem. Soc.* **2020**, *142*, 21469−21483.
(14) Guo, L. H.; Gao, H. Y.; Guan, Q. R.; Hu, H. B.; Deng, J. A.; Liu, J.; Liu, F. S.; Wu, Q. Substituent Effects of the Backbone in alpha-Diimine Palladium Catalysts on Homo- and Copolymerization of Ethylene with Methyl Acrylate. *Organometallics* **2012**, *31*, 6054−6062.
(15) Zhong, S. H.; Tan, Y. X.; Zhong, L.; Gao, J.; Liao, H.; Jiang, L.; Gao, H. Y.; Wu, Q. Precision Synthesis of Ethylene and Polar Monomer Copolymers by Palladium-Catalyzed Living Coordination Copolymerization. *Macromolecules* **2017**, *50*, 5661−5669.
(16) Poli, R. Relationship between one-electron transition metal reactivity and radical polymerization processes. *Angew. Chem., Int. Ed.* **2006**, *45*, 5058−5070.
(17) Poli, R. Organometallic Mediated Radical Polymerization. In *Polymer Science: A Comprehensive Reference*; Matyjaszewski, K., Möller, M., Eds.; Elsevier BV, 2012; Vol. *3*, pp 351−375.
(18) Poli, R. New phenomena in organometallic-mediated radical polymerization (OMRP) and perspectives for control of less active monomers. *Chem.—Eur. J.* **2015**, *21*, 6988−7001.
(19) Arvanatitopoulos, L. D.; Greuel, M. P.; Harwood, H. J. "Living" free radical photopolymerization using alkyl cobaloximes as photoinitiators. *Polym. Prepr.* **1994**, *35*, 549−550.
(20) Kermagoret, A.; Wenn, B.; Debuigne, A.; Jerome, C.; Junkers, T.; Detrembleur, C. Improved photo-induced cobalt-mediated radical polymerization in continuous flow photoreactors. *Polym. Chem.* **2015**, *6*, 3847−3857.
(21) Michalak, A.; Ziegler, T. DFT studies on the copolymerization of alpha-olefins with polar monomers: Ethylene-methyl acrylate copolymerization catalyzed by a Pd-based diimine catalyst. *J. Am. Chem. Soc.* **2001**, *123*, 12266−12278.
(22) Liu, Y.-S.; Harth, E. Distorted Sandwich α-Diimine PdII Catalyst: Linear Polyethylene and Synthesis of Ethylene/Acrylate Elastomers. *Angew. Chem., Int. Ed.* **2021**, *60*, 24107−24115.
(23) Grimme, S.; Antony, J.; Ehrlich, S.; Krieg, H. A consistent and accurate ab initio parametrization of density functional dispersion correction (DFT-D) for the 94 elements H-Pu. *J. Chem. Phys.* **2010**, *132*, 154104.
(24) Raju, R. K.; Bengali, A. A.; Brothers, E. N. A unified set of experimental organometallic data used to evaluate modern theoretical methods. *Dalton Trans.* **2016**, *45*, 13766−13778.
(25) Marenich, A. V.; Cramer, C. J.; Truhlar, D. G. Universal Solvation Model Based on Solute Electron Density and on a Continuum Model of the Solvent Defined by the Bulk Dielectric Constant and Atomic Surface Tensions. *J. Phys. Chem. B* **2009**, *113*, 6378−6396.
(26) Chen, L. Y.; Sanchez, D. R.; Zhang, B. F.; Carrow, B. P. "Cationic" Suzuki-Miyaura Coupling with Acutely Base-Sensitive Boronic Acids. *J. Am. Chem. Soc.* **2017**, *139*, 12418−12421.
(27) Walter, M. D.; White, P. S.; Brookhart, M. Synthesis, structure and computational studies of a cationic T-shaped Pd-complex. *New J. Chem.* **2013**, *37*, 1128−1133.
(28) Poli, R. A journey into metal-carbon bond homolysis. *C. R. Chim.* **2021**, *24*, 147−175.
(29) Michelas, M.; Fliedel, C.; Poli, R. Reversible Homolysis of Metal-Carbon Bonds. In *Comprehensive Organometallic Chemistry IV*; Elsevier, 2021; Vol. *1*, pp 31−85.
(30) Bamford, C. H.; Jenkins, A. D. Termination reaction in vinyl polymerization - Preparation of block copolymers. *Nature* **1955**, *176*, 78.
(31) Ayrey, G.; Humphrey, M. J.; Poller, R. C. Radiochemical studies of free-radical vinyl polymerizations. 7. Polymerization of methyl acrylate. *Polymer* **1977**, *18*, 840−844.
(32) Szablan, Z.; Junkers, T.; Koo, S. P. S.; Lovestead, T. M.; Davis, T. P.; Stenzel, M. H.; Barner-Kowollik, C. Mapping photolysis product radical reactivities via soft ionization mass spectrometry in acrylate, methacrylate, and itaconate systems. *Macromolecules* **2007**, *40*, 6820−6833.
(33) Ribelli, T. G.; Augustine, K. F.; Fantin, M.; Krys, P.; Poli, R.; Matyjaszewski, K. Disproportionation or Combination? The Termination of Acrylate Radicals in ATRP. *Macromolecules* **2017**, *50*, 7920−7929.
(34) Nakamura, Y.; Lee, R.; Coote, M. L.; Yamago, S. Termination Mechanism of the Radical Polymerization of Acrylates. *Macromol. Rapid Commun.* **2016**, *37*, 506−513.
(35) Ribelli, T. G.; Rahaman, S. M. W.; Matyjaszewski, K.; Poli, R. Catalyzed Radical Termination in the Presence of Tellanyl Radicals. *Chem.—Eur. J.* **2017**, *23*, 13879−13882.
(36) Thevenin, L.; Fliedel, C.; Matyjaszewski, K.; Poli, R. Impact of catalyzed radical termination (CRT) and reductive radical termination (RRT) in metal-mediated radical polymerization processes. *Eur. J. Inorg. Chem.* **2019**, 4489−4499.
(37) Schröder, K.; Konkolewicz, D.; Poli, R.; Matyjaszewski, K. Formation and Possible Reactions of an Organometallic Intermediate with Active Copper(I) Catalysts in an ATRP. *Organometallics* **2012**, *31*, 7994−7999.
(38) Ribelli, T. G.; Wahidur Rahaman, S. M.; Daran, J.-C.; Krys, P.; Matyjaszewski, K.; Poli, R. Effect of Ligand Structure on the CuII-R OMRP Dormant Species and its Consequences for Catalytic Radical Termination in ATRP. *Macromolecules* **2016**, *49*, 7749−7757.
(39) Ribelli, T. G.; Rahaman, S. M. W.; Matyjaszewski, K.; Poli, R. Catalyzed radical termination (CRT) in the metal-mediated polymerization of acrylates: experimental and computational studies. In *Reversible Deactivation Radical Polymerization: Mechanisms and Synthetic Methodologies*; Tsarevsky, N., Gao, H., Matyjaszewski, K., Sumerlin, B., Eds.; American Chemical Society, 2018; Vol. *1284*, pp 135−159.
(40) Fantin, M.; Lorandi, F.; Ribelli, T. G.; Szczepaniak, G.; Enciso, A. E.; Fliedel, C.; Thevenin, L.; Isse, A. A.; Poli, R.; Matyjaszewski, K. Impact of Organometallic Intermediates on Copper-Catalyzed Atom Transfer Radical Polymerization. *Macromolecules* **2019**, *52*, 4079−4090.

https://doi.org/10.1021/acs.organomet.3c00277
Organometallics 2023, 42, 2277−2286